Coupling Path Visualization and EMI Mitigation for Flyover QSFP Connectors

Atieh Talebzadeh , *Member, IEEE*, Pranay K. Vuppunutala, *Member, IEEE*, Kyoungchoul Koo, Hongyu Li , *Member, IEEE*, Jim Nadolny , Qian Liu, *Member, IEEE*, Jing Li , Kaustav Ghosh , Philippe C. Sochoux , Victor Khilkevich , *Member, IEEE*, James L. Drewniak , *Fellow, IEEE*, and David Pommerenke , *Fellow, IEEE*

Abstract—In this article, the energy parcels concept is used to reveal radiation physics and coupling in the entire structure of flyover quad form-factor pluggable (QSFP) interconnection. Flyover QSFP has better signal integrity than legacy surface mounted printed circuit board QSFP technology. To understand electromagnetic interference aspects, a simulation model was built and correlated to measured total radiated power (TRP) for common mode and differential mode excitations for a frequency range of 1-40 GHz. Further, the energy parcels and their trajectories concept were applied to visualize the coupling path by tracking back the energy parcels from outside of the chassis (quiet side) toward a host board inside the chassis (noisy side). Then, high-density regions of energy parcel trajectories guide where to place the absorbing material efficiently and appropriately. Two locations were examined by filling them with electromagnetic lossy material and improvement was validated by TRP simulation and measurement.

Index Terms—Coupling path, electromagnetic interference (EMI) mitigation, EMI/EMC, energy parcel, quad form-factor pluggable (QSFP) interconnect, reverberation chamber, total radiated power (TRP).

I. INTRODUCTION

LYOVER quad form-factor pluggable (QSFP) interconnection is considered a novel technology for 56+Gbps applications due to the fact that the legacy QSFP interconnection suffers from high insertion loss of printed circuit board (PCB) traces at millimeter-wave frequencies (e.g., 40 GHz). However, in flyover technology, these PCB traces are substituted with lower loss twinax cables. Twinax cables, referred to as "flyover cables," flyover the lossy PCB traces. This new approach

Manuscript received November 4, 2018; revised March 20, 2019 and July 23, 2019; accepted September 13, 2019. Date of publication October 22, 2019; date of current version August 13, 2020. (Corresponding author: Atieh Talebzadeh.)

A. Talebzadeh, P. K. Vuppunutala, K. Koo, Q. Liu, J. Li, K. Ghosh, V. Khilkevich, J. L. Drewniak, and D. Pommerenke are with the EMC Laboratory, Missouri University of Science and Technology, Rolla, MO 65401 USA (e-mail: ath27@mst.edu; pv6zf@mst.edu; kook@mst.edu; iqpg4@mst.edu; jlkc9@mst.edu; kgkb4@mst.edu; khilkevichv@mst.edu; drewniak@mst.edu; david.pommerenke@ieee.org).

- H. Li is with Broadcom Inc., Irvine, CA 92620 USA (e-mail: leo.li@broadcom.com).
- J. Nadolny is with Samtec Inc., Erie, PA 16506 USA (e-mail: jim. nadolny@samtec.com).
- P. C. Sochoux is with Juniper Networks, Inc., Sunnyvale, CA 94089 USA (e-mail: psochoux@juniper.net).

Color versions of one or more of the figures in this article are available online at http://ieeexplore.ieee.org.

Digital Object Identifier 10.1109/TEMC.2019.2943290

inherently offers several advantages than the legacy solution including more system design flexibility, higher density port configuration (multiple stack), improved thermal management, reduction in fabrication cost due to lower layer count PCBs, and improved material options [1]. To enable the flyover QSFP applicable in the networking industry, electromagnetic interference (EMI) aspects must be well understood. Further, the EMI impact of twinax cables penetrating the EMI cage, which houses the QSFP module, must be assessed.

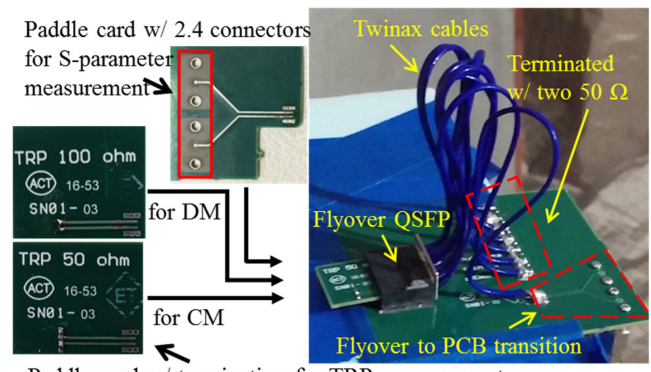
EMI associated with high-speed, high-density interconnections was studied including board-to-board interconnections (i.e., small form-factor pluggable (SFP) and QSFP) in [2]–[4], edge-coupled PCB backplane connectors in [5]–[9], and EMI shielding cage for legacy QSFP interconnections in [10]. The interconnections contribute to radiation emission at high frequencies. However, the coupling mechanism and the radiation physics in the entire structure of system were hardly completely understood [11]–[13]. Monitoring the surface current is known as the primary way to reveal the radiation physics and it is challenging for a complex structure. Besides, extracting the radiation currents from the surface current needs to obtain and analyze the characteristic mode [14].

In a previous study [1], the signal integrity (SI) and EMI performances of flyover QSFP were measured and compared with the legacy QSFP approach. In this article, a simulation model correlated to measurement is given based on time domain reflectometer (TDR) and total radiated power (TRP) measured results. The simulation model includes the EMI shielding cage and the correlation to measured TRP is verified with both differential mode (DM) and common mode (CM) excitations for the frequency range of 1-40 GHz. To understand the possible coupling paths, the concept of energy parcels to electromagnetic waves is used [15], [16]. This method has advantages from monitoring the surface currents as it reveals the radiation mechanism in an entire system but does not need to distinguish between the radiating and non-radiating currents. High density regions of energy parcel trajectories guide where to place the absorbing material efficiently and appropriately. Two locations were examined by filling them with electromagnetic lossy material and improvement was validated by TRP simulation and measurement.

In the following section, the simulation model is introduced and the correlation to measured TDR and TRP is discussed. In

0018-9375 © 2019 IEEE. Personal use is permitted, but republication/redistribution requires IEEE permission.

See https://www.ieee.org/publications/rights/index.html for more information.



Paddle card w/ termination for TRP measurement

Fig. 1. Test vehicles for flyover QSFP.

Section III, the energy parcels concept is illustrated using well-understood examples. Here, the emphasis lies on the difference between the visualization of the power flow from the Tx port and the tracked back energy parcels that had reached to the Rx port and are tracked back to their source to illustrate the path they took. The goal of this article is first to use the energy parcels idea to illustrate the coupling path in the entire structure of high-speed networking interconnects, from a host board inside the chassis to an Rx port outside of the chassis. By tracking back the energy parcels from the quiet side toward the noisy side (i.e., Rx to Tx), the coupling path is revealed. Second, the density of the parcels streamlines is considered to find the optimum location for EMI absorber to mitigate EMI from flyover QSFP. Simulation and measurement result show a possible path for reducing the EMI, which is presented in Section IV.

II. SIMULATION MODEL FOR FLYOVER QSFP

High-speed channel interconnects include several impedance discontinuities at their connectors and assemblies which act as an effective source of EM radiation. The flyover QSFP system also has several discontinuities at the interface between a module board and flyover QSFP connector at the host board, flyover QSFP connector to twinax cable, and twinax cable to direct connects cable connector right before IC. The EMI from those sources should be properly investigated and improved to meet the regulation before the design cycle completion. A simulation model for flyover QSFP is introduced for EMI characterization of flyover QSFP. Once the model achieves the correlation to measurement, it enables to perform simulation-based analysis.

A. Time Domain Reflectometer

The differential TDR response was obtained based on single-ended four-port S-parameters measurement. To perform the measurement, a test vehicle was designed and fabricated as shown in Fig. 1 that includes 15 cm twinax cables. One differential channel out of eight available channels in the QSFP interconnect was considered for the test. The rest of the channels were terminated in two 50 Ω resistors. As shown in Fig. 1, three paddle cards were designed and fabricated. The paddle card with two 2.4 mm launch connectors was used for four-port

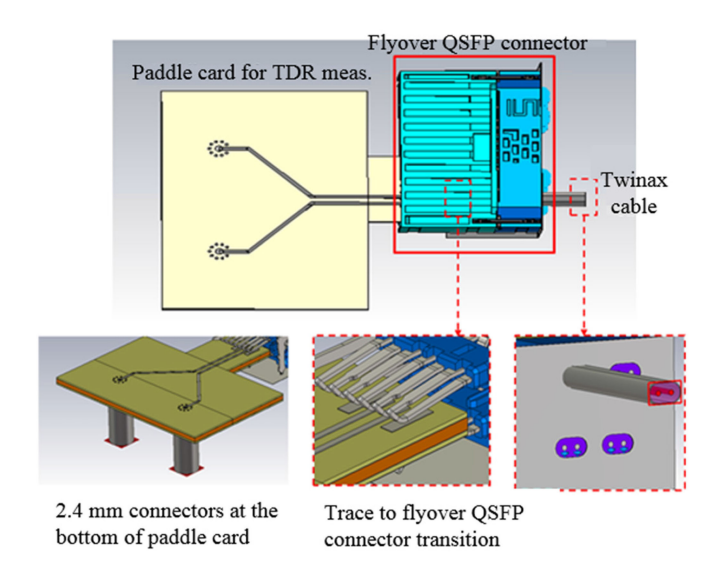


Fig. 2. Simulation model for TDR measurement in CST microwave studio.

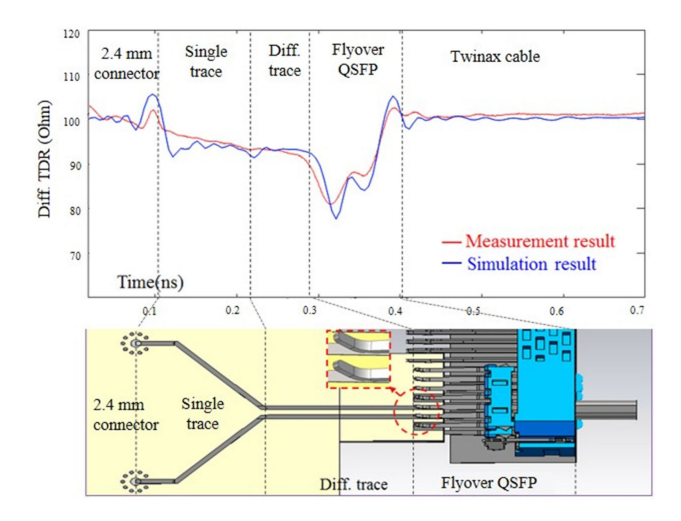
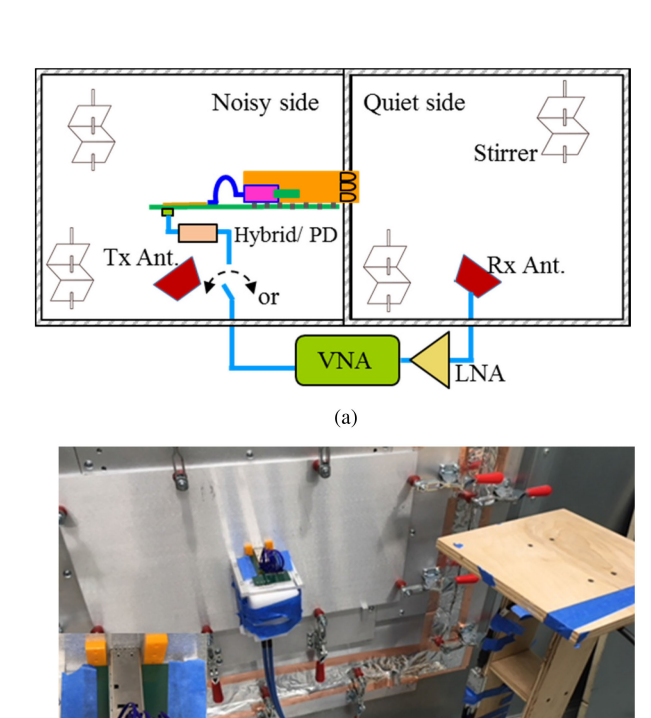


Fig. 3. Comparison between simulated TDR and measured TDR.

S-parameters measurement to obtain differential TDR impedance. The four-port S-parameter measurement was obtained for the frequency range of 10–40 GHz. The paddle cards with 50 Ω and 100 Ω terminations were used in the TRP measurements for the CM and DM setups, respectively.

Fig. 2 shows the simulation model with the paddle card for S-parameter measurement in CST microwave studio [17]. The model only includes 2.4 mm launch ports in the paddle card to the middle of twinax cable after the flyover QSFP connectors to reduce the simulation time. Therefore, the comparison between the simulation and measurement is only valid up to the twinax cable. The comparison between measured and simulated differential TDR responses is shown in Fig. 3 with the marked discontinuities for each signal path transition. A decent correlation between measurement and simulation is achieved. Several discontinuities are seen on the differential current path. The differential impedance of the single trace and differential (Diff.) traces for TDR measurement is lower than $100~\Omega$ because of the fabrication tolerance in trace thickness and design constraints.



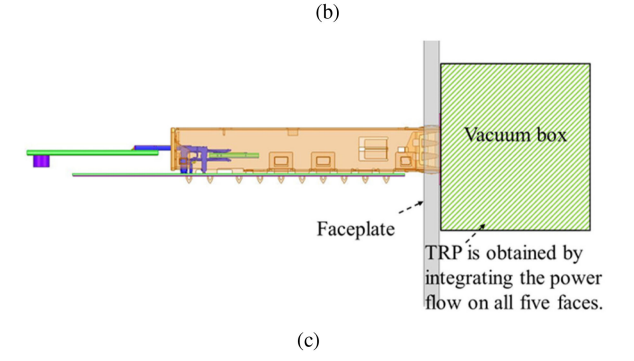


Fig. 4. Description of the test set-up using a dual reverberation chamber in (a) schematic, (b) actual set-up, and (c) simulation model in CST microwave studio.

Although the path differential impedance is less than ideal, full functionality was achieved.

B. TRP

To reveal the coupling path in flyover QSFP with the shielding cage, the TRP result for CM and DM was measured using a dual reverberation chamber for the frequency range of 1–40 GHz, as the set-ups display in Fig. 4(a) and (b). The well-known TRP substitution method [18], [19] was used to obtain TRP values. A paddle card plugged into a flyover QSFP with 50 and 100 Ω terminations for the CM and DM setups, respectively shown in Fig. 1. A simulation model was also created in CST microwave studio including the faceplate and a vacuum box for calculating the TRP on five surfaces, as shown in Fig. 4(c). This method was first presented in [20] to calculate TRP. The cables and the

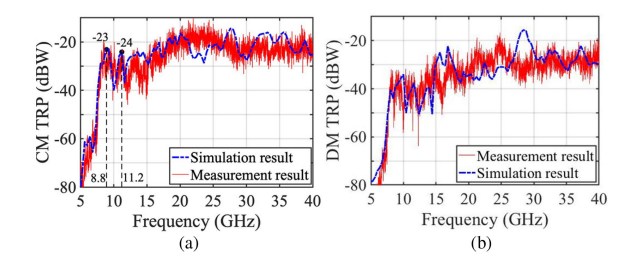


Fig. 5. TRP comparison between simulation and measurement in (a) CM, and (b) DM set-up.

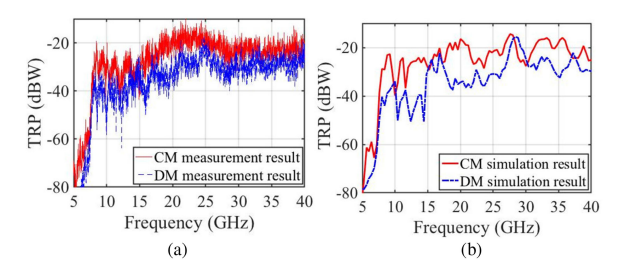


Fig. 6. TRP comparison between DM and CM excitations in (a) measurement and (b) simulation.

hybrid/power divider (PD) loss, as well as the loss of twinax cable, have been removed from the TRP measured results, as previously described in [1].

The TRP comparison between simulation and measurement for CM and DM set-ups are shown in Fig. 5. There is a little discrepancy between the simulation and measurement results at high frequencies, which can be because of the lack of high frequency material properties for the simulation model, eliminating the skew between the cablings and hybrid/PD in the simulation model, and the uncertainty of the de-embedding process to get the loss of the cable and hybrid/PD from the TRP measured results. The TRP from CM excitation is greater than the DM excitation, as the measured and simulation results for these two modes are compared in Fig. 6(a) and (b), respectively.

To reveal the coupling mechanism in the flyover QSFP interconnection, the CM excitation was considered at two peak frequencies of 8.8 and 11.2 GHz, as marked in Fig. 5(a). Then, the energy parcels method was used to understand the coupling mechanism.

III. COUPLING MECHANISM IN FLYOVER QSFP USING ENERGY PARCELS

Understating of the EM coupling in electronic devices is a challenge for EMC engineers [21], [22]. Several methods have been established to visualize the EM coupling including ray-tracing [23], [22], diffuse scattering [24], [23], and reaction theorem [25]. However, visualization of the EM coupling based on energy parcels and their trajectories [15], [16] is a powerful and relatively easy tool to address the coupling path in the entire structure of flyover QSFP interconnection.

To illustrate the idea, two examples are presented. The baseline includes two dipole antennas (Tx and Rx) placed at a λ

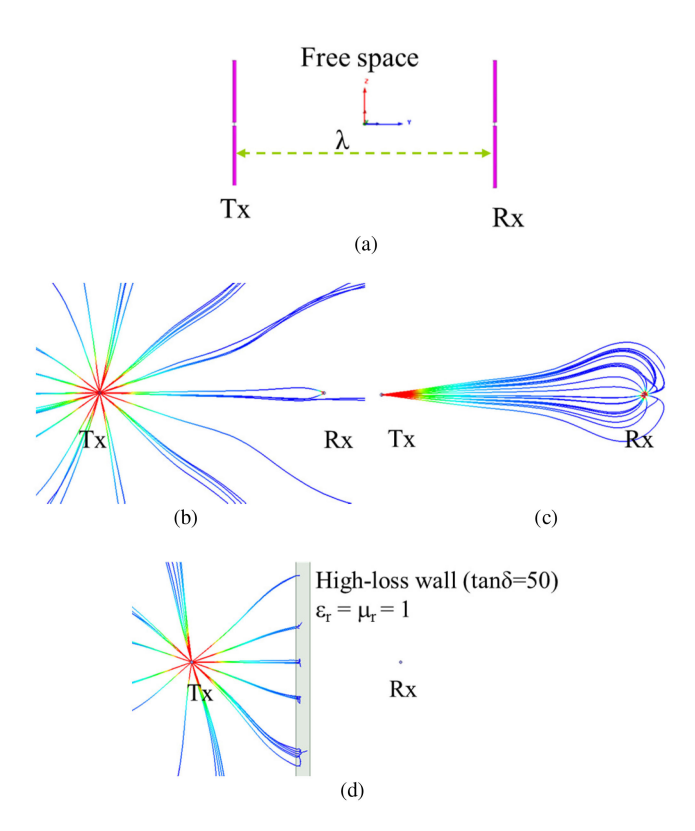


Fig. 7. Example of two antennas. (a) Antennas placement in free space. (b) Power flow energy parcels starting at the Tx. (c) Tracked back energy parcels from the Rx, which reach the Tx. (d) Power flow energy parcels from the Tx at the presence of a high-loss wall.

distance as shown in Fig. 7(a). Only the transmitter antenna is excited. Plotting the streamlines of the real part of the Poynting vector at the Tx antenna port shows the power flow of energy parcels propagates in space from the Tx antenna, as displayed in Fig. 7(b). Some energy parcels are reached at the Rx antenna. To obtain the energy path from the Tx to the Rx antenna, the trajectories are tracked back from the Rx antenna. To this end, the streamlines of the real part of the Poynting vector along with a negative sign (the negative sign is needed for the purpose of tracking back) are plotted at the Rx antenna port. Fig. 7(c) shows the tracked back energy parcels at the Rx antenna. In Fig. 7(d), a high-loss wall is placed between two antennas with a dielectric loss coefficient of 50. The relative permittivity and permeability are considered as one. The transmitted energy parcels (power flow) are shown in Fig. 7(d). As seen, the energy parcels are absorbed in the lossy wall and as a result, no EM energy can reach to the Rx antenna (i.e., no tracking back of the energy parcels from the Rx antenna is possible in this case). As shown, there is a difference between the power flow from the Tx port and tracking back the energy parcels from the Rx port. The first one shows the propagation of energy in free space and in all directions. However, the second one specifically shows the coupling path between the Tx and Rx. Tracking back the energy parcels from the Rx port is a convenient way to visualize the EM energy coupling paths and understand the physics associated with the EM problems.

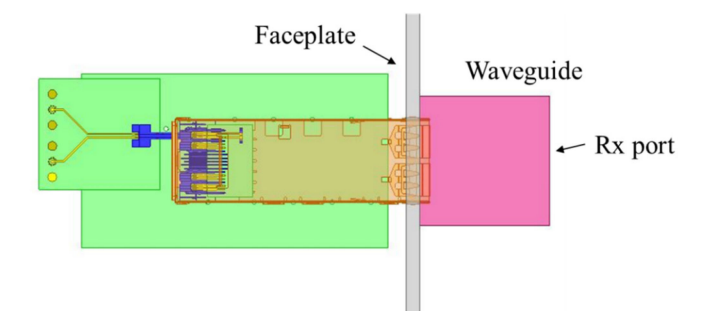


Fig. 8. Simulation model for applying energy parcels in flyover QSFP.

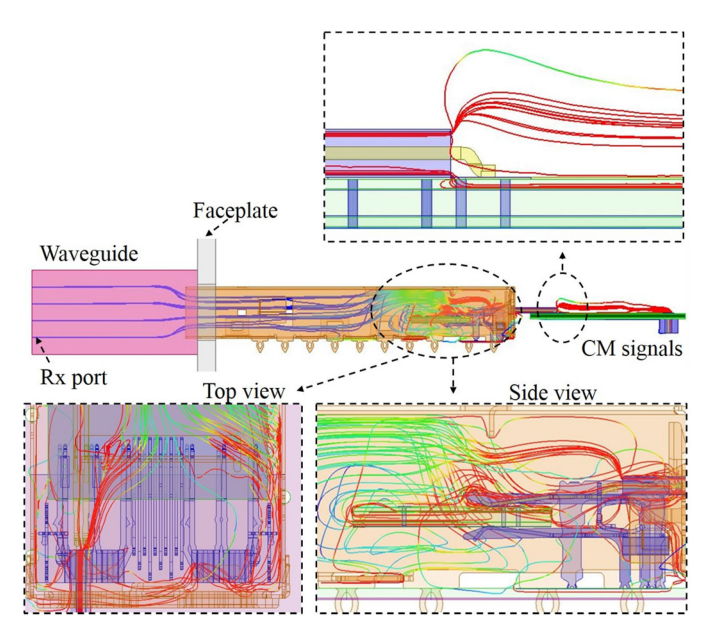


Fig. 9. Energy parcels streamlines tracked from the flyover interconnect to the waveguide on the quiet side of the faceplate at the frequency of 8.8 GHz.

A. Application for EMI Coupling Path in Flyover QSFP

To reveal the coupling mechanism in the entire structure of flyover QSFP interconnection, the CM excitation is considered at two frequencies of 8.8 and 11.2 GHz, as the TRP is maxima at these frequencies. A simulation model was built in HFSS [26] including the faceplate. To track back the energy parcels, a receiver antenna should be located after the faceplate. To be independent to the receiver antenna location, a waveguide antenna was designed located on the faceplate, but on the quiet side as shown in Fig. 8.

The energy parcels are collected at the receiver port of the waveguide antenna. The cut off frequency of the waveguide is about 7 GHz. Fig. 9 shows the tracked back energy parcels trajectories plotted at the *Rx* port (the waveguide port on the quiet side) at the frequency of 8.8 GHz.

The streamlines indicate the number of energy parcels received from the flyover QSFP interconnection at the waveguide port on the quiet side. At the transition of the signal traces on the PCB host board to the twinax cables, zoomed in on the top right of the figure, energy parcels enter the twinax cable. Some of them are due to the radiation of launch 2.4 mm connectors. Some others enter the twinax cable from the ground layer of the

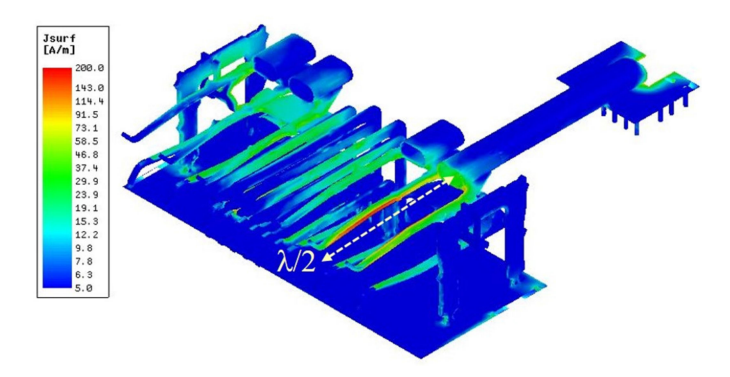


Fig. 10. Surface current distribution on the ground pins at the frequency of $8.8\,\mathrm{GHz}.$

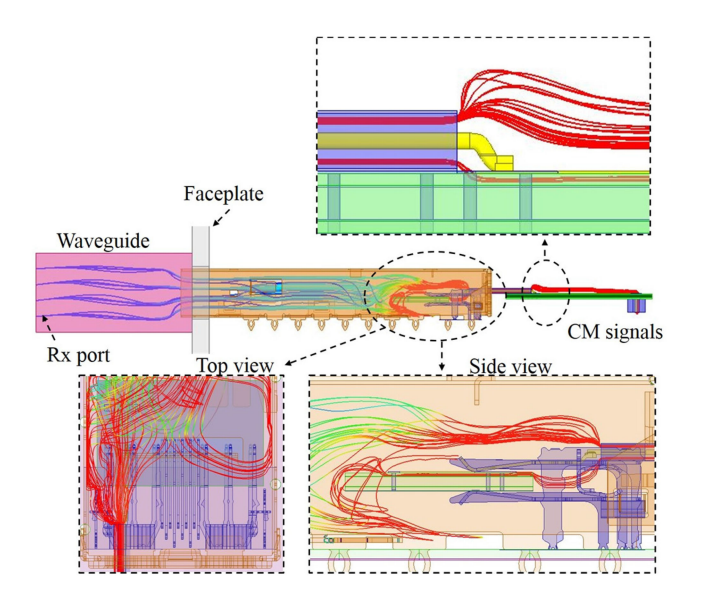


Fig. 11. Energy parcels streamlines tracked from the flyover interconnect to the waveguide on the quiet side of the faceplate at the frequency of 11.2 GHz.

host PCB; these are the CM currents that excite the EMI cage and radiate from it. Inside the cage, the energy parcels are dense around the transition from the QSFP signal pins to the traces on the paddle card PCB. This discontinuity contributes to the excitation of the EMI shielding cage. In addition, the energy parcels are dense around the ground pins of the flyover QSFP.

The EMI investigation [5] reports that the ground pin of the SFP connector resonates as a $\lambda/2$ antenna at the frequency of 8 GHz. This is shown based on the surface current density of the ground pins. Because of the SFP and QSFP are related, similar resonances are to be expected. For this purpose, the surface current on the ground pins of the flyover QSFP is shown in Fig. 10. The $\lambda/2$ antenna element is marked in the figure. However, the advantage of using the energy parcels concept is that we can visualize the coupling path in the entire structure. Furthermore, an effective area to place absorber material can be recognized by determining areas of dense parcels streamlines.

The coupling path at the frequency of 11.2 GHz is also interesting because the TRP value is maxima at this frequency, which is marked in Fig. 5(a). The energy parcel trajectories collected at the Rx port are shown in Fig. 11. More energy parcels enter the twinax cable from the launch connectors at this frequency and

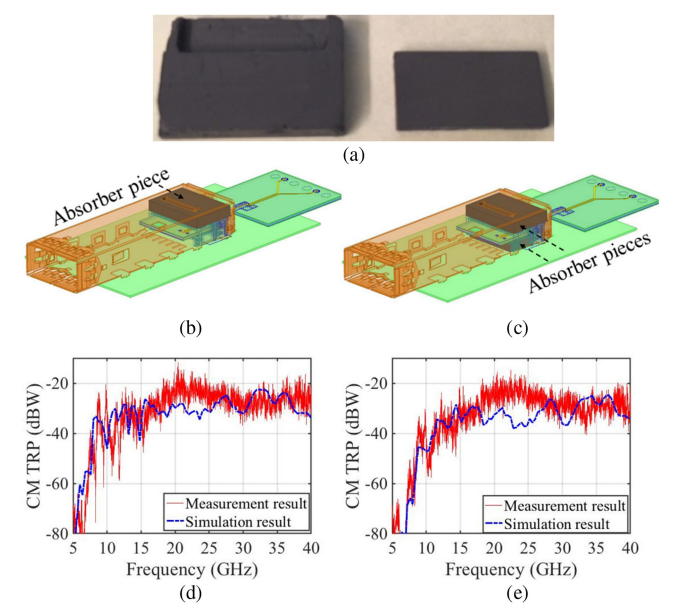


Fig. 12. (a) Lossy pieces made for the measurement. (b) Simulation model for lossy material on top of the connector. (c) Simulation model for lossy material on top and the bottom of the connector. (d) Measured and simulated CM TRP results for the lossy material on top of the connector. (e) Measured and simulated CM TRP results for the lossy material on top and the bottom of the connector.

directly contribute in the excitation of the EMI shielding cage and reach to the receiver port. In addition, the return current enters the cage from the ground layer of the host PCB. Inside the cage, these energy parcels go through the ground layer of the paddle card PCB. Some of the energy parcels are damped at the two 50 Ω terminations. The rest contribute to the excitation of the cage and reach the waveguide port (i.e., the Rx antenna) at the other side of the faceplate. Therefore, the paddle card PCB and termination resistors are the dominant sources at this frequency. The energy parcels concept is an easy way to reveal and visualize the coupling mechanism in the entire of a complex structure at different frequencies. In this article, this concept was applied at two frequencies of 8.8 and 11.2 GHz for CM excitation, but this method can be used for further frequencies and different structures. Usually, the surface current distribution is used to understand the resonance structure, which can be complex and complicated because the surface current includes both radiating and non-radiating current. To distinguish between the radiating and non-radiating current, the characterization modes of the structure [6] needs to be solved.

IV. APPLYING EMI MITIGATION TECHNIQUES

To mitigate the EMI associated with the flyover interconnection, a thermoplastic, polyamide-based, and hot melt magnetic absorber was used to make proper pieces. From the energy parcel trajectories at the frequency of 8.8 GHz, the top of the connector is a dense area with the energy parcels. Further, the trajectory of the energy parcels at the frequency of 11.2 GHz shows that the bottom area, in addition to the top, is a dense area of energy parcels. Thus, two pieces of lossy material were fabricated to be placed on the top and bottom of the connector, as shown in Fig. 12(a). Two tests were performed when absorbing pieces were placed only at the top, and both top and bottom

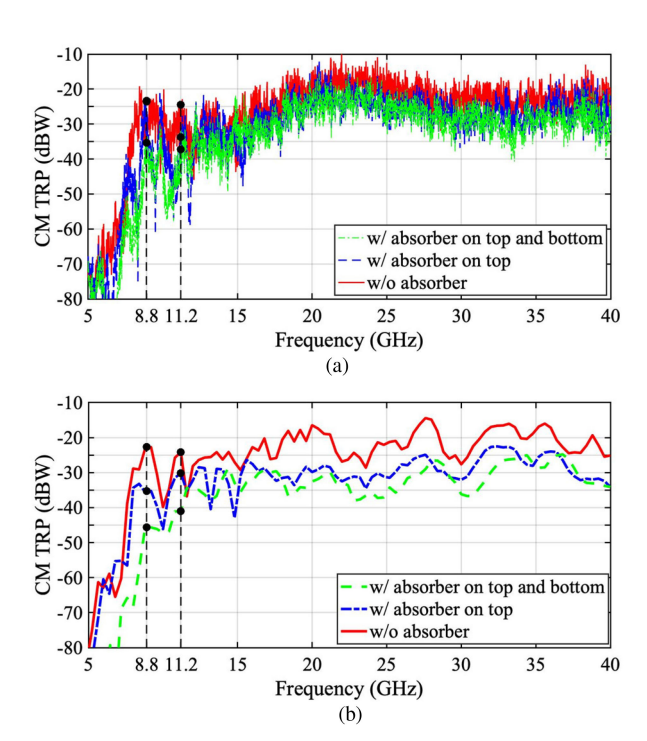


Fig. 13. CM TRP comparison between using and not using absorbers for (a) measurement, (b) simulation.

of the connector. Fig. 12(b) shows the simulation model for the case that the absorber piece was placed only on the top of the connector. The TRP simulation and measurement results for CM excitation are compared in Fig. 12(d). The discrepancies between the measurement and simulation can be because of the (inevitable) inaccuracy during the fabrication process of the absorber pieces and the modeling process of the material properties in the simulation. In the fabrication process, the absorb filament was melted in a designed aluminum mold using a hot glue gun. More than 10 dB improvement achieved at the frequency of 8.8 GHz, from the simulation results. For the second case, the absorber pieces were placed on the top and the bottom of the interconnection. Fig. 12(c) and (e) shows the simulation model and the TRP results for CM excitation. Placing the absorber material on top and the bottom of the connector is very effective to reduce the TRP. For example, ~20 dB and \sim 10 dB improvements were obtained from the simulation at the frequency of 8.8 and 11.2 GHz, respectively.

Fig. 13(a) compares measured CM TRP for the case without the absorber, with the absorber on the top, and with the absorber on the top and the bottom of the flyover QSFP interconnect. Fig. 13(b) compares the simulation data. Applying the lossy material at both locations (i.e., the top and the bottom), is more effective with a 20 dB improvement from 7 to 12 GHz and about a 5 dB improvement at frequencies greater than 12 GHz.

When the absorber pieces were placed on the top/bottom of the connector, discrepancies between the measured data and the simulation are observed. These discrepancies can be a result of the (inevitable) inaccuracy of the hand-made absorber pieces during the fabrication process. In the fabrication process, the absorber filament was melted into a small aluminum mold using

TABLE I TRP Comparison W/ and W/o Absorber in Measurement and Simulation

Frequency	8.8 GHz		11.2 GHz	
TRP (dBW)	Meas.	Sim.	Meas.	Sim.
w/o absorber	-23.3	-23.2	-24.5	-24.1
Top absorber	-23.6	-35.6	-33.7	-32.3
Top/bottom absorber	-35.4	-46.1	-37.2	-35.2

a hot glue gun. Thus, having air bobbles in the fabricated samples are possible. However, in the simulation model, the absorber was modeled homogeneously. Also, the frequency-dependent electrical properties (i.e., the primitivity and permeability with real and complex components) were included in simulation model. A comparison of the TRP values at the frequencies of 8.8 GHz and 11.2 GHz are given in Table I.

V. CONCLUSION

Flyover technology is designed as a new solution for 56+ Gbps applications. In this article, the energy parcels concept is used to reveal the coupling mechanism in the entire structure. A simulation model was created in HFSS and CM excitation was selected. The energy parcels were tracked back from the quiet side of faceplate at two frequencies of 8.8 and 11.2 GHz. Form the simulated streamlines at 8.8 GHz, it was observed that two coupling mechanisms occur, which are related to the launch connectors on the host PCB as well as the return current due to discontinuity at the flyover QSFP pins to the paddle card. At 11.2 GHz, it was also observed that two coupling mechanisms occur, which are related to the launch connectors on the host PCB as well as the 50 Ω terminations at the paddle card. To mitigate the EMI, EM absorbers can be applied at areas in which the streamline are dense (i.e., top and bottom of the connector). Finally, two pieces of lossy material were built to be placed on the top and bottom of the flyover QSFP. The simulation and measurement with decent correlation show greater than 10 dB improvement from 7 to 12 GHz and ∼5 dB improvement at frequencies greater than 12 GHz.

ACKNOWLEDGMENT

The authors gratefully acknowledge G. Biddle from Samtec Inc. for providing helpful discussions for the shielding aspects of QSFP and flyover QSFP topologies.

REFERENCES

- A. Talebzadeh et al., "SI and EMI performance comparison of standard QSFP and flyover QSFP connectors for 56+ Gbps applications," in Proc. IEEE Int. Symp. Electromagn. Compat. Signal/Power Integrity, 2017, pp. 776-781.
- [2] J. Li and J. Fan, "Radiation physics and design guidelines of high-speed connectors," *IEEE Trans. Electromagn. Compat.*, vol. 58, no. 4, pp. 1331– 1338, Aug. 2016.

- [3] J. Zhou and H. Runjing, "High-speed SFP+ signal integrity simulation and measurement," *J. Commun. Comput.*, vol. 11, pp. 371–377, 2014.
- [4] J. Li et al., "EMI coupling paths and mitigation in a board-to-board connector," *IEEE Trans. Electromagn. Compat.*, vol. 57, no. 4, pp. 771–779, Aug. 2015.
- [5] B. Archambeault, S. Connor, M. Halligan, J. Drewniak, and A. Ruehli, "Electromagnetic radiation resulting from PCB/high-density connector interfaces," *IEEE Trans. Electromagn. Compat.*, vol. 55, no. 4, pp. 614–623, Aug. 2013.
- [6] H. Chen, S. Connor, T. Wu, and B. Archambeault, "The effect of various skew compensation strategies on mode conversion and radiation from highspeed connectors," in *Proc. IEEE Int. Symp. Electromagn. Compat.*, 2013, pp. 328–332.
- [7] X. Tian et al., "Quantifying radiation and physics from edge-coupled signal connectors," *IEEE Trans. Electromagn. Compat.*, vol. 57, no. 4, pp. 780– 787, Aug. 2015.
- [8] H. Chen et al., "Investigation of the radiated emissions from high-speed/high-density connectors," IEEE Trans. Electromagn. Compat., vol. 58, no. 1, pp. 220–230, Feb. 2016.
- [9] M. Halligan, X. Tian, X. Li, S. Connor, D. Beetner, and J. Drewniak, "Quantifying high-density connector radiation in a lossy multisignal environment," *IEEE Trans. Electromagn. Compat.*, vol. 58, no. 1, pp. 270–277, Feb. 2016.
- [10] A. Talebzadeh, P. C. Sochoux, J. Li, Q. Liu, K. Ghosh, and D. Pommerenke, "Shielding effectiveness, coupling path, and EMI mitigation for QSFP cages with heatsink," *IEEE Trans. Electromagn. Compat.*, vol. 60, no. 5, pp. 1254–1262, Oct. 2018.
- [11] C. Hsiao et al., "Radio-frequency interference mitigation strategies for high-speed connectors," in Proc. IEEE Elect. Des. Adv. Packaging Syst. Symp., 2013, pp. 56–59.
- [12] J. Li, S. Toor, A. Bhobe, J. Drewniak, and J. Fan, "Radiation physics and EMI coupling path determination for optical links," in *Proc. IEEE Int. Symp. Electromagn. Compat.*, 2014, pp. 576–581.
- [13] L. Zhang et al., "EMI coupling paths and mitigation in optical transceiver modules," *IEEE Trans. Electromagn. Compat.*, vol. 59, no. 6, pp. 1848– 1855, Dec. 2017.
- [14] Y. Cao, Y. Wang, L. Jiang, A. Ruehli, J. Fan, and J. Drewniak, "Quantifying EMI: A methodology for determining and quantifying radiation for practical design guidelines," *IEEE Trans. Electromagn. Compat.*, vol. 59, no. 5, pp. 1424–1432, Oct. 2017.
- [15] H. Li, V. Khilkevich, and D. Pommerenke, "Identification and visualization of coupling paths—Part II: Practical application," *IEEE Trans. Electromagn. Compat.*, vol. 56, no. 3, pp. 630–637, Jun. 2014.
- [16] H. Li, V. Khilkevich, and D. Pommerenke, "Identification and visualization of coupling paths—Part I: Energy parcel and its trajectory," *IEEE Trans. Electromagn. Compat.*, vol. 56, no. 3, pp. 622–629, Jun. 2014.
- [17] "CST Studio Suite 2017," Computer Simulation Technology AG, 2017.
- [18] H. Krauthauser, "On the measurement of total radiated power in uncalibrated reverberation chambers," *IEEE Trans. Electromagn. Compat.*, vol. 49, no. 2, pp. 270–279, May 2007.
- [19] Testing and Measurement Techniques Reverberation Chamber Testing Methods, IEC Standard 6100-4-21, 2003.
- [20] X. Zhou, J. Li, H. Fan, A. Bhobe, P. Sochoux, and J. Yu, "High-frequency EMC design verification through full-wave simulations and measurements in reverberation chamber," in *Proc. IEEE Int. Symp. Electromagn. Com*pat., 2013, pp. 299–305.
- [21] S. Shinde, X. Gao, K. Masuda, V. V. Khilkevich, and D. Pommerenke, "Modeling EMI due to display signals in a TV," *IEEE Trans. Electromagn. Compat.*, vol. 58, no. 1, pp. 85–94, Feb. 2016.
- [22] S. Shinde et al., "Radiated EMI estimation from DC-DC converters with attached cables based on terminal equivalent circuit modeling," *IEEE Trans. Electromagn. Compat.*, vol. 60, no. 6, pp. 1769–1776, Dec. 2017.
- [23] T. Kurner, D. Cichon, and W. Wiesbeck, "Concepts and results for 3D digital terrain-based wave propagation models: An overview," *IEEE J. Sel. Areas Commun.*, vol. 11, no. 7, pp. 1002–1012, Sep. 1993.
- [24] V. Degli-Esposti, D. Guiducci, A. de'Marsi, P. Azzi, and F. Fuschini, "An advanced field prediction model including diffuse scattering," *IEEE Trans. Antennas Propag.*, vol. 52, no. 7, pp. 1717–1728, Jul. 2004.
- [25] J. Malmstrom, H. Henrik, and B. Jonsson, "On mutual coupling and coupling paths between antennas using the reaction theorem," *IEEE Trans. Electromagn. Compat.*, vol. 60, no. 6, pp. 2037–2040, Dec. 2018.
- [26] ANSYS, HFSS, Software, ANSYS Inc., Canonsburg, PA, USA, 2017.



Atieh Talebzadeh (M'18) received the B.S. degree from Shahed University, Tehran, Iran, in 2010, the M.S. degree from the Amirkabir University of Technology, Tehran, Iran, in 2013, and the Ph.D. degree from the Electromagnetic Compatibility Laboratory, Missouri University of Science and Technology, Rolla, MO, USA, in 2018, all in electrical engineering.

In 2017, she was a Co-Op Student in the EMC Design Group, Juniper Networks, Sunnyvale, CA, USA. In 2018, she joined Apple Inc., as an EMC

design engineer. Her research interests include numerical and experimental study of EMI in high-speed interconnections, visualizing coupling paths by energy parcels approach, EMI mitigation, ESD system level, sparkles electrostatic discharge, and analyzing the triboelectric charging.

Dr. Talebzadeh was the recipient of the Dean's Ph.D. Scholar Award in 2017, Technical Paper Award of ASHRAE Annual Conference PR Material in June 2016, and the first place of IEEE EMC/SI Student Hardware Design Competition in August 2016.



Pranay Vuppunutala (S'16–M'19) received the B.S. degree in electronics and communication engineering from Jawaharlal Nehru Technological University, Hyderabad, India, in 2015 and the M.S. degree in electrical engineering from the Missouri University of Science and Technology, Rolla, MO, USA, in 2019.

He is currently with Cisco systems as a Signal and Power Integrity Engineer in Enterprise Access Switching division. His research interests include signal integrity, system level power distribution network design, and electromagnetic compatibility.



Kyoungchoul Koo received the B.S., M.S., and Ph.D. degrees in electrical engineering, in 2006, 2008, and 2012, respectively, from KAIST, Daejeon, South Korea.

From 2012 to 2016, he worked at Samsung Electronics and Developed Design Methodology for on/off-chip PI co-optimization in mobile SoCs. From 2016 to 2017, he worked at EMC group in Missouri S&T, as a Visiting Research Assistant Professor. In 2017, he joined Apple Inc., Cupertino, CA, USA, where he currently a Senior Signal/Power Integrity

Engineer.

Dr. Koo was the recipient of the Best Paper Award at DesignCon 2014 and EDAPS 2015 and the Best Student Paper Award at EMC Compo 2011 and EMC 2011(2nd runner up).



Hongyu Li (S'09–M'12) received the Ph.D. degree in electrical engineering from the Missouri University of Science and Technology, Rolla, MO, USA, in 2012.

From 2005 to 2008, he was an Application Engineer with STMicroelectronics, Shanghai, China. Since 2011, he has been a Signal Integrity Engineer with Broadcom Inc., Irvine, CA, USA. His research interests include signal integrity, power integrity and electromagnetic interference in high-speed IC package and system.



Jim Nadolny received the M.S. degree in electrical engineering from the University of New Mexico, NM, USA, in 1992. He is active within the technical community currently serving as a Technical Group chairman for IEEE P370, a standard focused on precision measurements of passive interconnect components. He is a frequent presenter at DesignCon with Best Paper awards in 2004, 2008, 2012, 2018 and has more than 25 peer reviewed publications. At Samtec, he tracks technology trajectories via industry standards, MSAs and other collaborations.



Philippe C. Sochoux received the B.S. and M.S. degrees in electrical engineering from Marquette University, Milwaukee, WI, USA, in 1990 and 1994, respectively.

In 2014, he joined Juniper Networks, where he is currently a Senior Manager for EMC Design. Prior to joining Juniper, he managed functions including EMC, Mechanical DVT, Optical DVT, Safety, NEBS and Signal Integrity at Cisco Systems.

Victor Khilkevich, photograph and biography not available at the time of publication.



Qian Liu (M'13) received the B.S. degree in electrical engineering from the University of Electronic Science and Technology of China, Chengdu, China, in 2013, and the master's degree in electrical engineering from Electromagnetic Compatibility Lab, Missouri University of Science and Technology, MO, USA, in 2016.

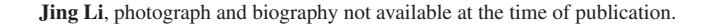
In 2015, she was a Co-Op in EMC design center of IBM system group, Raleigh, NC, USA. After graduation, she worked in the EMC design group in Juniper Network, Sunnyvale, CA, USA, from 2016

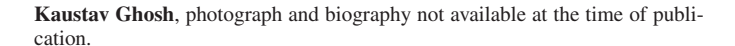
to 2019. She is currently an EMC design Engineer with Apple Inc., Cupertino, CA, USA. Her research interests include electromagnetic modeling, absorber lossy material, RF interference and EMI issues on PCBs.



James L. Drewniak (F'06) received the B.S., M.S., and Ph.D. degrees in electrical engineering from the University of Illinois at Urbana-Champaign, Champaign, IL, USA.

He is a Curator's Professor of electrical and computer engineering with Missouri S&T, Rolla, MO, USA. His research interests include electromagnetic compatibility, signal and power integrity, and electronic packaging.







David Pommerenke (F'15) received the Diploma in 1996 and the Ph.D. degree from the Technical University Berlin, Berlin, Germany, in 1996.

After working at Hewlett Packard for five years, he joined the Electromagnetic Compatibility Laboratory with the Missouri University of S&T in 2001 and became CTO of ESDEMC in July 2019. He has authored or coauthored more than 200 papers and is inventor on 13 patents. His main research interests include measurement/instrumentation ESD, electronic design and EMC.

Dr. Pommerenke is an Associated Editor for the IEEE TRANSACTIONS ON EMC